Green Science

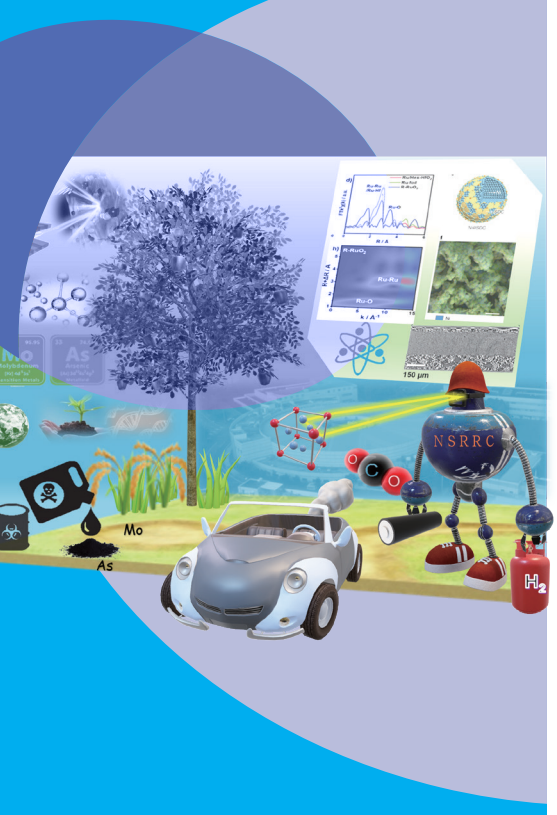

The NSRRC serves as a critical hub for advanced scientific investigation, providing researchers with state-of-the-art, high-resolution tools to address urgent environmental and energy challenges. The studies featured in this year's Green Science section demonstrate how synchrotron X-ray techniques, including spectroscopy, imaging, and three-dimensional microscopy, enable unprecedented insights into complex biological, chemical, and structural phenomena. In 2025, many researchers using NSRRC facilities achieved significant breakthroughs in green sciences. Due to space limitations, this section highlights five notable contributions. These investigations cover environmental remediation, clean energy conversion, and next-generation energy storage, reflecting a comprehensive and interdisciplinary approach to global sustainability.

In the field of environmental detoxification, innovative strategies have been developed to mitigate toxic element contamination. A study led by Yen-Lin Cho and Yu-Ting Liu used extremophilic red microalgae to immobilize arsenic in oxygen-depleted groundwater environments. By integrating X-ray absorption spectroscopy (XAS), X-ray fluorescence nanoprobe mapping, and transmission X-ray microscopy, they clarified a bio-oxidative mechanism in which the algae promote iron oxidation, leading to the formation of reactive Fe^{3+} hydroxides that effectively sequester arsenite. In a significant study by Puu-Tai Yang and Shang-Li Wang, the environmental and agricultural impacts of industrial molybdenum (Mo) discharge were systematically examined using quick-scanning XAS. Their work demonstrated how soil pH and texture govern Mo speciation and its bioavailability, influencing Mo accumulation in wheat grains and identifying potential pathways for human health risk.

Another aspect of green sciences, advances in catalytic science, further support the global pursuit of carbon neutrality and sustainable fuel production. *Operando/in situ* XAS was employed to monitor the real-time structural and electronic evolution of single-atom catalysts during CO_2 reduction reactions, led by Hao Ming Chen. The measurements challenged conventional paradigms by demonstrating that catalytic efficiency is governed by dynamic electronic adaptability rather than static atomic configurations. In parallel, efforts toward industrial-scale CO_2 conversion focused on the thermal stability and durability of core–shell nanocatalysts headed by Xile Hu, which were shown to retain high energy efficiency under extreme operating temperatures. In addition, hydrogen production was addressed through studies on the hydrogen spillover effect by two research teams, Qi Shao and B. J. Hwang, in which XAS and near-ambient-pressure X-ray photoelectron spectroscopy revealed how phase and interface engineering can significantly enhance hydrogen generation kinetics. Looking toward the future of energy storage, Ying Shirley Meng and his collaborators investigated all-solid-state batteries using nondestructive three-dimensional imaging. Projection X-ray microscopy enabled direct visualization of the internal architecture of pouch cells, allowing quantitative assessment of porosity evolution, interfacial contact loss, and ion-transport tortuosity during electrochemical cycling. These insights provide critical guidance for the rational design of more robust, high-capacity, and industry-ready energy storage systems.

Together, the studies featured in this section underscore the essential role of NSRRC beamlines in linking atomic- and electronic-scale dynamics with macroscopic performance and practical applications. These reinforce NSRRC's contribution to advancing green science and promoting a more sustainable future. (by Chi-Liang Chen)

Extremophile Algae Power Arsenic Cleanup

Cyanidiophyceae can detoxify and immobilize arsenic under oxygen-free conditions.

Arsenic contamination in groundwater poses severe health risks worldwide, especially in regions where anaerobic (oxygen-depleted) conditions promote the dissolution of toxic arsenite [As(III)]. Conventional treatment methods often struggle in these reducing environments. A new study published in *Chemical Engineering Journal* demonstrates a promising biological method using extremophilic red microalgae (Cyanidiophyceae) to bio-oxidize iron and immobilize arsenic under anaerobic conditions.[1] The research led by Yu-Ting Liu (National Chung Hsing University) and Yen-Lin Cho (National Sun Yat-sen University), in collaboration with scientists from the NSRRC, reveals that Cyanidiophyceae species *Cyanidium caldarium* (Cc) and *Galdieria partita* (Gp) can oxidize ferrous iron [Fe(II)] to ferric iron [Fe(III)] anaerobically, forming reactive Fe(III) (oxyhydr)oxides that efficiently trap arsenic. These findings open a new route for biological arsenic remediation in oxygen-depleted environments such as aquifers and sediments. To elucidate how these extremophilic algae achieve such efficient detoxification, the team employed a suite of synchrotron-based techniques, including X-ray absorption spectroscopy (XAS) at **TLS 17C1** and **TPS 44A**, X-ray fluorescence (XRF) nanoprobe mapping at **TPS 23A**, transmission X-ray microscopy (TXM) at **TLS 01B1**, and Fourier-transform infrared (FTIR) microspectroscopy at **TLS 14A1**.

Under strictly anaerobic conditions, both Cc and Gp were able to convert over 96.8% of sorbed Fe(II) into Fe(III) within hours. The resulting Fe(III) hydroxides served as active sites for arsenite adsorption and coprecipitation. When pre-loaded with Fe, the algae showed 45–61% higher As(III) sorption capacity compared with unmodified cells,

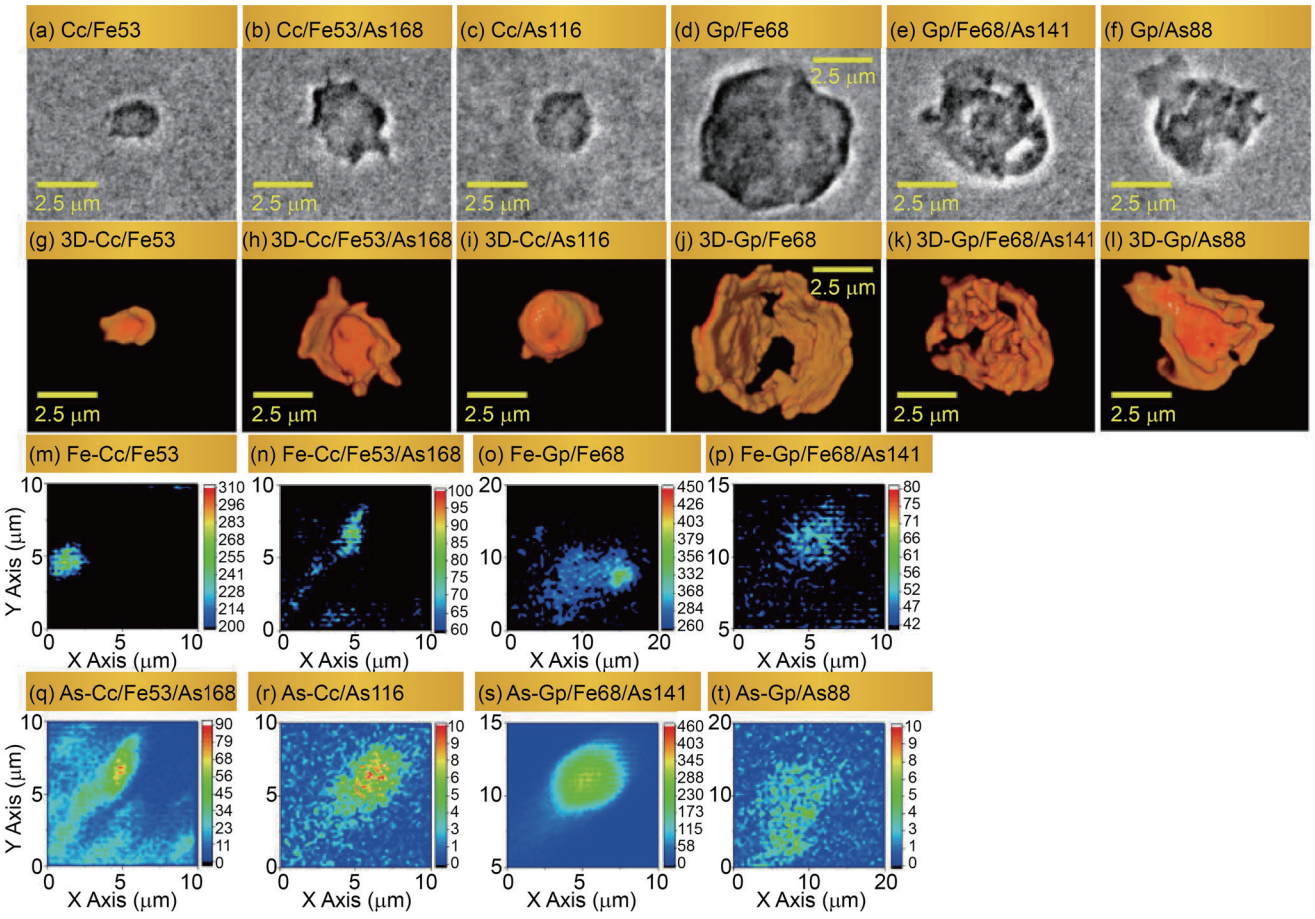

Fig. 1: (a–f) 2D images, (g–l) 3D tomography images, (m–p) Fe distribution, and (q–t) As distribution in Cc, Gp, and Fe-loaded Cc and Gp collected during Fe(II) sorption kinetics experiments and upon acquisition of As(III) sorption isotherms. The numbers after Fe and As indicate the sorption amounts in mg g^{-1}. The distributions of Fe and As metals in the 2D and 3D images were shown as darker and lighter areas, respectively. The specific Fe and As distributions (m–t) in cells were determined by nano (XRF) mapping. [Reproduced from Ref. 1]

achieving up to 168 mg g^{-1} arsenic uptake—far exceeding most inorganic sorbents under similar conditions. XAS analysis confirmed that these Fe(III) phases were primarily amorphous hydroxides and Fe–polysaccharide complexes, both known for high affinity toward arsenic. The Fe–As association observed by XRF mapping demonstrated that Fe localized along the cell periphery, while As was distributed across cell walls and interiors, indicating cooperative surface and intracellular processes.

Despite similar Fe oxidation abilities, the two microalgae displayed distinct arsenic detoxification pathways, as revealed by synchrotron XAS and FTIR spectroscopy. Cc utilized an intracellular detoxification mechanism. In Cc, XAS identified As(III)–cysteine complexes [As(III)–cys] formed inside cells, while FTIR showed structural protein changes (altered α-helix/β-strand ratios), confirming biochemical adaptation to metal stress. This strategy allowed Cc to internalize and stabilize arsenic within the cytoplasm. By contrast, Gp adopted a surface-mediated oxidation mechanism. Fe(II) bio-oxidation and As(III) oxidation to less toxic As(V) occurred concurrently, with the oxidized species bound to extracellular polysaccharides. This indicates that Gp relies on its cell-wall chemistry and extracellular enzymes for As detoxification.

Figure 1 presents the 3D tomography (TXM) and nano-XRF elemental mapping that directly reveal how Cc and Gp distribute Fe and As after Fe(II) loading and As(III) sorption. The Fe signal forms a clear ring around both Cc and Gp cells, demonstrating that Fe(II) taken up by the algae is rapidly oxidized at or near the cell wall. This visualizes the exact location where Fe(III) phases form under anaerobic conditions. Additionally, arsenic XRF signals overlap with Fe-rich zones, directly supporting the conclusion that newly formed Fe(III) minerals act as the dominant sinks for As(III). This co-localization provides spatial evidence that Fe(III) bio-oxidation is the key step enabling the high As uptake measured in the sorption experiments. In Gp, Fe and As signals remain largely at the cell surface, consistent with its surface-based As oxidation and extracellular polysaccharide binding. In Cc, arsenic signals penetrate deeper into the cell, supporting the intracellular As(III)–cysteine complexation pathway revealed by XAS and FTIR. By visually capturing Fe–As distribution at the single-cell level, Cyanidiophyceae enhance arsenic removal because their anaerobic Fe(II) bio-oxidation generates highly reactive Fe(III) phases that efficiently immobilize As(III).

This study demonstrates that Cyanidiophyceae can function as natural, self-regenerating bio-oxidizers capable of coupling iron cycling and arsenic immobilization even in oxygen-free systems—conditions typical of contaminated aquifers. By converting Fe(II) to Fe(III) and forming stable Fe(III) hydroxides that co-precipitate arsenic, the algae offer a sustainable route for *in-situ* groundwater cleanup. Moreover, their resilience, ease of cultivation, and micrometer-scale size enable practical recovery through simple microfiltration, making them viable for engineered treatment systems. The strong Fe–As binding confirmed by synchrotron XAS also ensures minimal risk of secondary metal release, further supporting their use in long-term environmental applications.

The combined biological and synchrotron findings highlight how extremophilic algae, armed with ancient iron-oxidizing genes, can be harnessed as eco-friendly bio-oxidizers for arsenic removal. Under anaerobic conditions, Cc and Gp exhibit complementary mechanisms that together create a highly effective, resilient system for As(III) detoxification. Through advanced X-ray spectroscopy and microscopy, the research team unveiled the hidden interplay between Fe redox cycling, As sequestration, and cellular adaptation. This research not only deepens our understanding of microbial metal metabolism but also showcases nature-inspired solutions for global water challenges. (Reported by Yu-Jong Wu)

This report features the work of Yen-Lin Cho, Yu-Ting Liu, and their co-workers published in Chem. Eng. J. ***523****, 168303 (2025).*

TPS 23A X-ray Nanoprobe
- XRF
- Materials Science, Soft Matters

TLS 01B1 X-ray Microscopy
- TXM
- Materials Science

TLS 14A1 IR Microscopy
- IR mapping
- Materials Science, Life science

TPS 44A Quick-scanning X-ray Absorption Spectroscopy

TLS 17C1 EXAFS
- XAS
- Materials Science

Reference

1. N. A. T. Than, L. C. Hsu, Y.-H. Chen, K. Huangmee, C.-C. Wang, H. Y. Teah, Y.-M. Tzou, Y.-L. Cho, Y.-T. Liu, Chem. Eng. J. **523**, 168303 (2025).

Soil Properties Control Molybdenum Uptake by Wheat

Anthropogenic sources of molybdate can be taken up by wheat plants, especially from alkaline soils.

Molybdenum (Mo) is a micronutrient and functions as a cofactor in enzymes in both plants and animals. While its concentrations in the natural environment are low, recent studies have shown elevated levels of Mo in soils and waters near industrial parks in Taiwan.[1] The discharge of Mo into nearby agricultural lands may lead to excessive accumulation in plants and pose potential health risks. For example, excessive intake of Mo can cause chlorosis, yellowing, and reduced productivity in plants, as well as copper deficiency in livestock. With the growing demand for semiconductors, it is necessary to elucidate how soil properties control the chemical speciation of Mo in soils and its accumulation in plants. However, due to the low concentration of Mo in natural soils, examining its chemical species remains challenging; thus, the information available from previous studies is limited.

A recent study by Puu-Tai Yang and Shan-Li Wang (National Taiwan University) investigated Mo uptake by wheat plants grown in three Taiwanese soils.[2] Using X-ray absorption spectroscopy at **TPS 44A**, the research group found that Mo occurred primarily as sorbed Mo(VI) and Ca- and Fe-Mo(VI) precipitates (**Fig. 1**). The relative abundance of the Mo(VI) species varied with soil texture and pH. In acidic soils (Pc: pH 4.4, silty clay loam; Tn: pH 4.9, silty loam), sorbed Mo(VI) was the dominant species, followed by Fe-Mo(VI), with the clay-rich soil (Pc) containing a higher ratio of sorbed Mo(VI). In the alkaline soil (pH 8.2, silty clay loam), Mo presented mainly as Ca-Mo(VI). The decreases in sorbed Mo(VI) and Ca-Mo(VI) during cultivation suggested their availability to wheat plants.

The accumulation of Mo in wheat plants was highest in the alkaline soil (**Fig. 2**, see next page), consistent with the greater decrease in sorbed Mo(VI) during cultivation (**Fig. 1**). This finding is supported by the group's previous work, which showed that maximum molybdate sorption by soils is negatively correlated with soil pH.[3] Less Mo sorbed onto soils at higher pH could therefore result in greater Mo availability to plants.

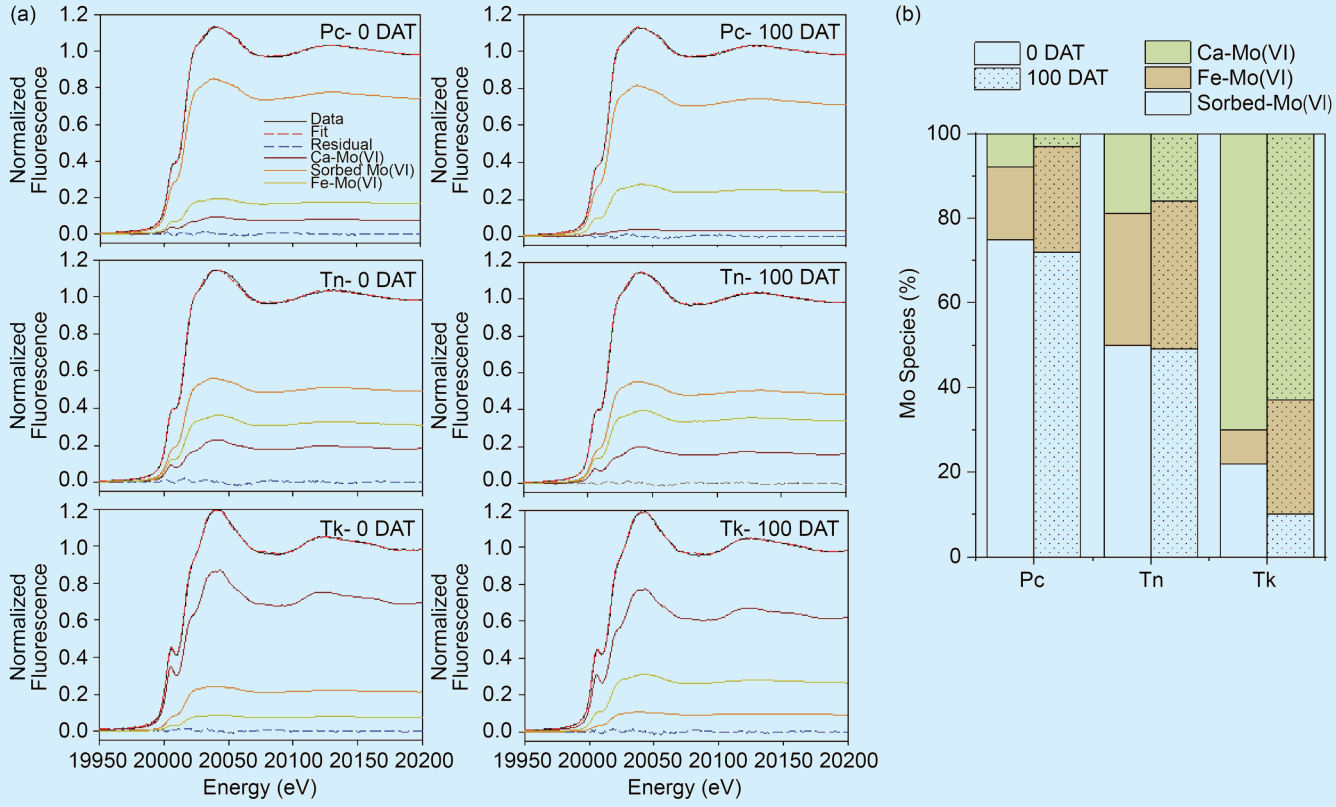

Fig. 1: Mo K-edge X-ray absorption near-edge structure spectra of Mo-spiked soil samples before (0 DAT) and after (100 DAT) wheat cultivation (a), and speciation determined by linear combination fitting (b). [Reproduced from Ref. 2]

In summary, the study demonstrated that the newly introduced Mo can significantly increase its concentration in wheat grain, posing a potential risk to human health. Identifying Mo species in soils using X-ray absorption spectroscopy provides valuable insight into the roles of soil properties in Mo accumulation in wheat plants. (Reported by Puu-Tai Yang, National Taiwan University)

This report features the work of Puu-Tai Yang and Shang-Li Wang published in J. Environ. Manage. ***374****, 124097 (2025).*

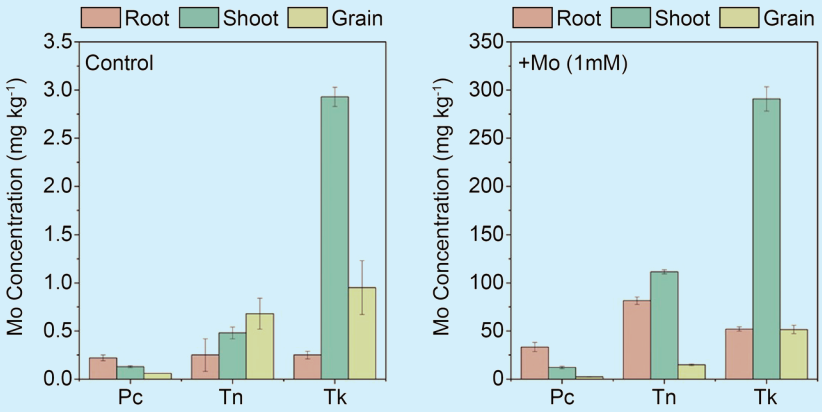

Fig. 2: Mo concentrations in the root, shoot, and grain of wheat plants grown in Pc, Tn, and Tk soils without (control) and with added Mo. [Reproduced from Ref. 2]

TPS 44A Quick-scanning X-ray Absorption Spectroscopy

- XAS
- Environmental Science, Soil Science, Chemistry

References

1. Y. W. Lin, T. S. Liu, H. Y. Guo, Y. T. He, Z. R. Lin, Review and Prospect of Agricultural Environmental Resources Protection in Taiwan, Taichung, Taiwan, 153 (2015, in Chinese).
2. P. T. Yang, S. L. Wang, J. Environ. Manage. **374**, 124097 (2025).
3. P. T. Yang, S. L. Wang, J. Hazard. Mater. **408**, 124934 (2021).

From Atomic Dynamics to Industrial Efficiency: New Pathways for CO_2 Conversion

Catalytic function is governed by atomic-scale motion and interfacial charge control. Synchrotron X-ray techniques reveal both, enabling researchers to connect microscopic dynamics with macroscopic stability.

Carbon dioxide sits at the center of one of humanity's greatest paradoxes. It sustains life by regulating Earth's temperature and feeding plants through photosynthesis—yet in excess, it threatens our climate, our oceans, and our future. As scientists race to build a carbon-neutral world, the ability to transform CO_2 from a waste gas into a renewable feedstock has become a defining challenge of modern chemistry. In the race toward carbon neutrality, two recent breakthroughs, one published in *Nature* and the other in *Journal of the American Chemical Society*, improve our understanding of CO_2 conversion activated by catalysts, from the transient dynamics of single atoms to the structural endurance of industrial-scale alloys. These works led respectively by Hao Ming Chen (National Taiwan University) and Xile Hu (École Polytechnique Fédérale de Lausanne, Switzerland) bridge the gap between atomic-level dynamics and industrial-scale performance. Together, they form a comprehensive view of how catalysts function, adapt, and endure in the fight against climate change.

In the study reported in *Journal of the American Chemical Society*,[1] Chen and his team developed a series of atomically dispersed transition-metal–nitrogen–carbon catalysts (M–N–C), in which individual metal atoms such as Mn, Fe, Co, Ni, or Cu are anchored by nitrogen atoms on a carbon support. Each catalyst consists of metal–nitrogen fourfold sites ($M–N_4$). These materials are widely studied for electrochemical CO_2 reduction, a process that uses electricity to convert CO_2 into carbon monoxide (CO), which can be further processed into fuels or industrial feedstocks. Despite their structural similarity, the catalysts exhibited very different activities. Nickel- and manganese-based M–N–C showed particularly high selectivity and efficiency for CO production, while others were less active. To determine why, the researchers turned to *operando* quick-scanning X-ray absorption spectroscopy performed at **TPS 44A**, which is capable of monitoring the structural evolution of single metal atoms under working electrochemical conditions in real time. The data revealed

that the most active catalysts undergo a reversible geometric change during CO_2 reduction. Under applied potential, an extra oxygen atom temporarily coordinates to the metal center, creating a five-coordinate ($M–N_4–O$) configuration. When the potential is removed, the site returns to its original four-coordinate state. This dynamic structural change occurs repeatedly during operation.

Computational analysis showed that this transient coordination affects the electronic structure of the metal, stabilizing a half-occupied dz^2 orbital that promotes CO_2 activation and facilitates CO release. This dynamic site, rather than a static configuration, is responsible for the high catalytic activity, as shown in **Fig. 1**. This finding overturns a common assumption in catalysis that a stable, unchanging structure is always best. Instead, a catalyst's flexibility and ability to reorganize electronically under reaction conditions can be the key to efficiency.

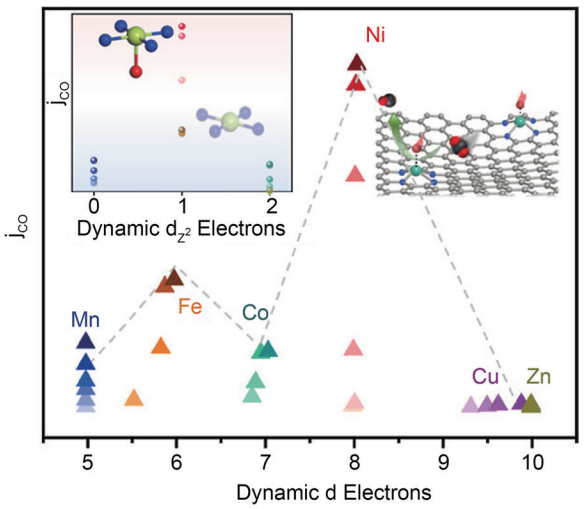

Fig. 1: Correlation between CO production current density (j_{CO}) and the number of dynamic d electrons for atomically dispersed $M–N_4$ catalysts (M = Mn, Fe, Co, Ni, Cu, Zn) during CO_2 electroreduction. Synchrotron-based time-resolved X-ray absorption spectroscopy revealed that the catalytic activity increases with the presence of a half-occupied dynamic dz^2 orbital, which facilitates optimal CO_2 adsorption and CO desorption. Among the series, $Ni–N_4$ exhibits the highest j_{CO} due to its pronounced dynamic dz^2 electron behavior, as illustrated by the inset showing transient structural distortion and CO_2 activation on the $Ni–N_4$ site. [Reproduced from Ref. 1]

While single-atom catalysts operate efficiently at room temperature, industrial CO_2 conversion often takes place under far more extreme conditions, such as in high-temperature solid oxide electrolysis cells. At 800 °C or higher, most materials lose structure or sinter into inactive forms. Achieving both high activity and long-term stability in such environments is a major challenge. In the study published in *Nature*,[2] Hu and his collaborators designed a core–shell nanocatalyst that meets these demands. Their material, composed of a $Co_{0.5}Ni_{0.5}$ alloy core encapsulated by a samarium-doped ceria (Sm_2O_3–CeO_2, SDC) shell, was engineered to maintain structural integrity and chemical reactivity during high-temperature operation. The Co–Ni@SDC catalyst exhibited outstanding performance for CO_2 electrolysis, maintaining 90% energy efficiency and 1 A cm^{-2} current density for more than 2,000 hours. This achieves an unprecedented level of durability for such systems. The oxide shell plays several critical roles: it protects the alloy from oxidation, prevents particle agglomeration, and facilitates oxygen ion transport across the interface.

To verify how the material behaves during its long lifetime, the team employed synchrotron X-ray absorption spectroscopy (XAS) measurements at multiple beamlines, including those at NSRRC's **SP 12B1** —the Taiwan-contract beamline

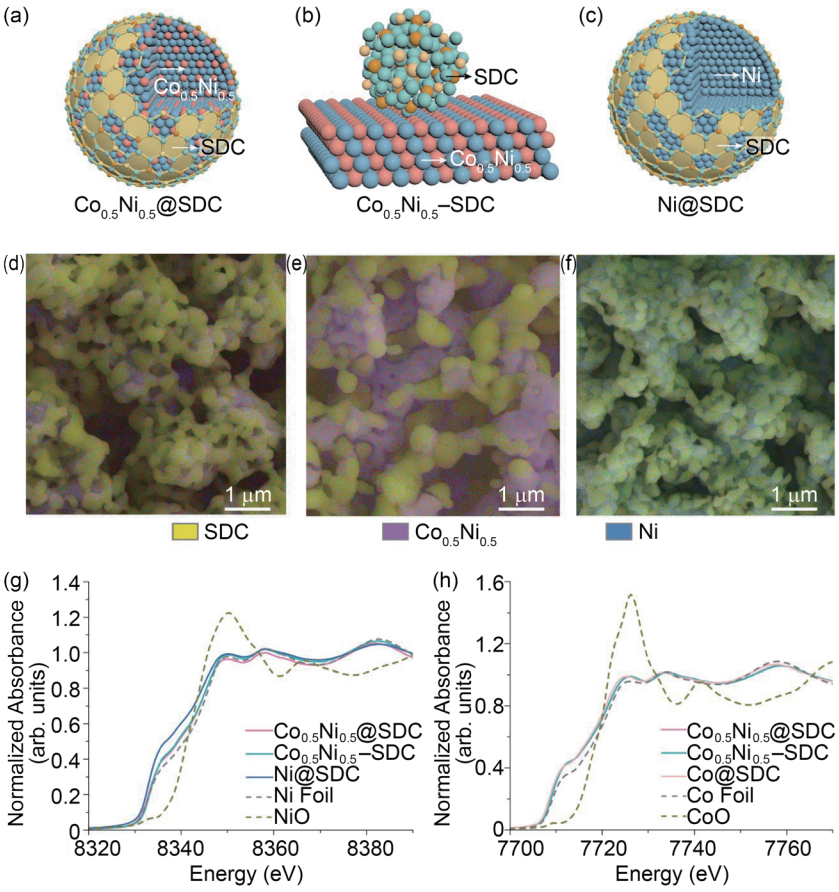

Fig. 2: Schematic illustrations of (a) $Co_{0.5}Ni_{0.5}$@SDC, (b) $Co_{0.5}Ni_{0.5}$–SDC, and (c) Ni@SDC catalysts. Merged scanning electron microscopy and energy-dispersive X-ray spectroscopy mappings for (d) $Co_{0.5}Ni_{0.5}$@SDC, (e) $Co_{0.5}Ni_{0.5}$–SDC, and (f) Ni@SDC catalysts. (g) Ni K-edge XANES spectra and (h) Co K-edge XANES spectra. [Reproduced from Ref. 2]

at SPring-8 in Japan—PETRA III, and the Australian synchrotron. XAS provides detailed information about atomic coordination and electronic states, even under elevated temperatures. The results showed that the alloy core retained its metallic Co–Ni bonding, while the ceria shell remained crystalline and stable, as shown in **Fig. 2**. Crucially, interfacial charge transfer was detected between the metal and the oxide: electrons moved from the Co–Ni core to the CeO_2 lattice, partially reducing Ce^{4+} to Ce^{3+} and creating oxygen vacancies. These vacancies serve as active sites for CO_2 adsorption and activation, while the metallic core promotes electron transfer for CO formation. This dual-site mechanism, verified by *operando* X-ray photoelectron spectroscopy (XPS) and density functional theory calculations, explains both the catalyst's high activity and its resistance to degradation. The interface acts as a self-regulating system, continuously balancing charge and maintaining structural stability under harsh conditions.

Although the above-mentioned studies focus on different systems, they tell a consistent story about how CO_2 conversion can be optimized. In both cases, the key lies in understanding the relationship between structure, electronic behavior, and reaction environment, and synchrotron X-rays make that understanding possible. At the atomic scale, X-ray spectroscopy revealed that catalytic activity emerges from the dynamic adaptation of electronic orbitals during reaction. At the macroscopic scale, high-energy X-ray and XPS analyses demonstrate that long-term durability arises from controlled charge transfer across interfaces. Together, these insights form a continuous picture of how catalysts must behave: responsive enough to activate CO_2 efficiently, yet stable enough to operate for thousands of hours. Furthermore, both studies highlight the growing importance of *operando* (*in situ*, under working conditions) measurements. Traditional "before-and-after" characterization provides only static images, missing the transient phenomena that govern real catalytic behavior. Synchrotron radiation, with its intense and tunable X-rays, allows scientists to collect structural and electronic information directly during reaction, bridging the gap between laboratory design and practical performance.

Overall, these findings redefine how researchers design materials for CO_2 utilization. In low-temperature electrochemical systems, understanding dynamic orbital behavior helps identify active configurations and design catalysts that can adapt under applied potentials. In high-temperature systems, insights into interfacial charge flow and oxygen vacancy formation enable the creation of long-lasting reactors suitable for industrial deployment. The implications extend beyond CO_2 conversion. The same principles are applicable to water splitting, ammonia synthesis, hydrocarbon reforming, and any reaction in which the interplay between electrons, atoms, and surfaces determines efficiency. The combined use of synchrotron spectroscopy, theoretical modeling, and materials engineering is now recognized as a cornerstone of modern catalysis research. (Reported by Yu-Jong Wu)

This report features the works of Hao Ming Chen, Xile Hu, and their collaborators published in J. Am. Chem. Soc. ***147****, 13027 (2025) and Nature* ***641****, 1156 (2025).*

TPS 44A Quick-scanning X-ray Absorption Spectroscopy
SP 12B1 Materials X-ray Study

- XAS
- Materials Science

References

1. J. Wang, H. Y. Tan, C.-S. Hsu, Y.-C. Chu, C.-W. Chan, K.-H. Chen, X.-R. Lin, Y.-C. Lee, H.-C. Chen, H. M. Chen, J. Am. Chem. Soc. **147**, 13027 (2025).
2. W. Ma, J. Morales-Vidal, J. Tian, M.-T. Liu, S. Jin, W. Ren, J. Taubmann, C. Chatzichristodoulou, J. Luterbacher, H. M. Chen, N. López, X. Hu, Nature **641**, 1156 (2025).

Hydrogen Spillover-Driven Hydrogen Evolution Reaction *via* Heterointerface and Catalyst Phase Engineering

Tailoring materials that promote the hydrogen spillover effect is crucial for effectively controlling hydrogen atoms during the electrocatalytic hydrogen generation.

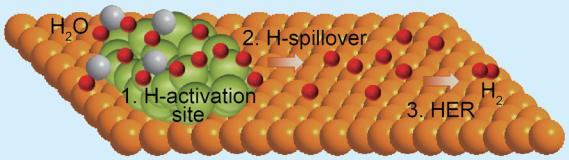

Fig. 1: The schematic diagram of the hydrogen spillover process.

Hydrogen spillover is an important interfacial phenomenon that regulates the behavior of hydrogen atoms in hydrogen-mediated catalytic conversion processes and hydrogen storage technologies. However, the hydrogen spillover effect (HSPE) is highly structure-dependent, and substrates with certain compositions are typically unfavorable. Therefore, selecting an appropriate substrate is crucial for effectively triggering hydrogen spillover. Qi Shao (Soochow University, China) and his team demonstrated that tuning the substrate's phase structure can transform spillover-inactive substrates into spillover-active ones.[1] Their work revealed that metastable hexagonal phase hafnium oxide (Hex-HfO_2) significantly enhances hydrogen spillover, whereas the conventional monoclinic phase (M-HfO_2) is spillover-inactive. The higher Gibbs free energy and distinct structural and bonding characteristics of metastable phases make them promising candidates for effectively triggering the HSPE. Their study systematically explored the hydrogen spillover phenomenon by uniformly dispersing ruthenium (Ru) nanoclusters on two types of 2D layered hafnium oxides, a metastable phase (Ru/Hex-HfO_2) and a stable phase (Ru/M-HfO_2). The occurrence of hydrogen spillover in these materials was assessed using multiple approaches, including colorimetric tests, hydrogen temperature-programmed desorption (H_2-TPD), and activity degradation evaluation with chemical probes. Electronic state characterization by X-ray photoelectron spectroscopy (XPS) revealed that Hex-HfO_2 has a higher Hf valence state than M-HfO_2. Additionally, the Hf 4f spectra of Ru/Hex-HfO_2 suggested electron transfer from Hex-HfO_2 to the Ru clusters. The X-ray absorption near-edge structure (XANES) and extended X-ray absorption fine structure (EXAFS) measurements (**Fig. 2**) were conducted at the **TPS 44A** beamline of the NSRRC. The XANES spectra showed a stronger white-line peak at the Hf L-edge for Hex-HfO_2 compared to M-HfO_2, indicating a higher oxidation state of hafnium in the metastable phase. These

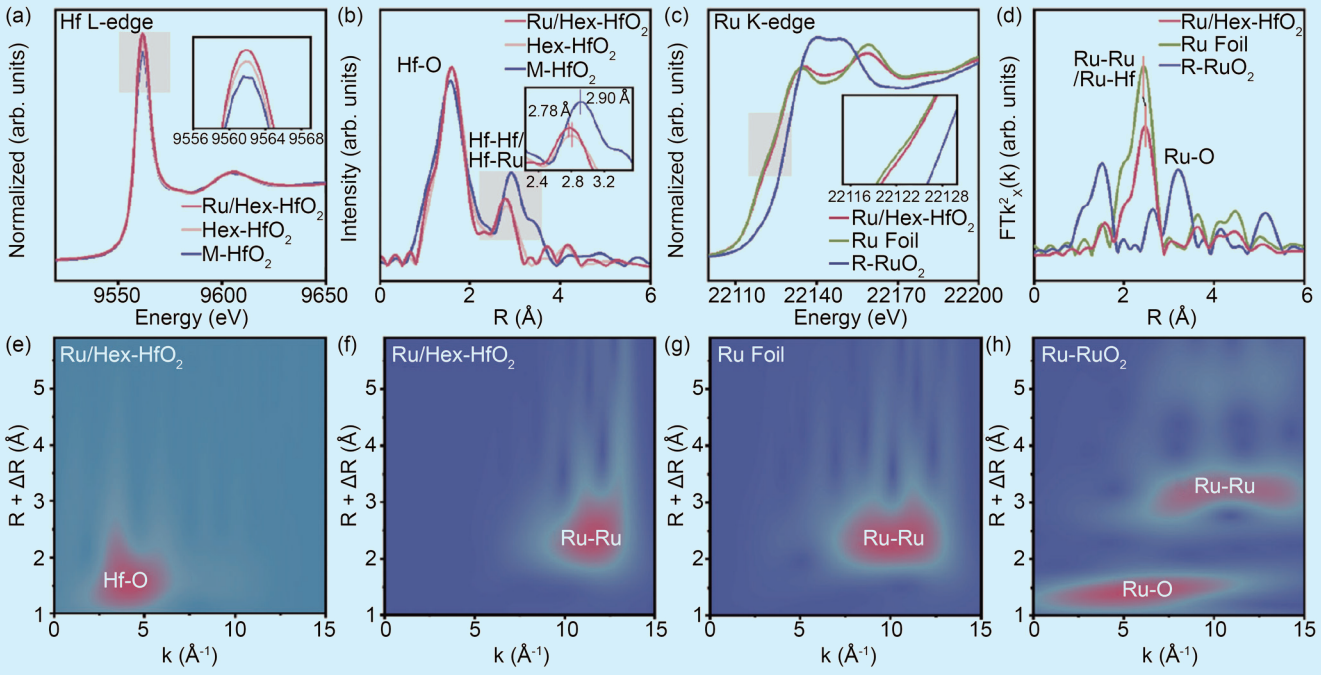

Fig. 2: (a) Hf L-edge spectra; (b) FT-EXAFS spectra; (c) Ru K-edge spectra; (d) FT-EXAFS spectra; (e) Hf L-edge WT-EXAFS; and (f–h) Ru K-edge WT-EXAFS of the materials. [Reproduced from Ref. 1]

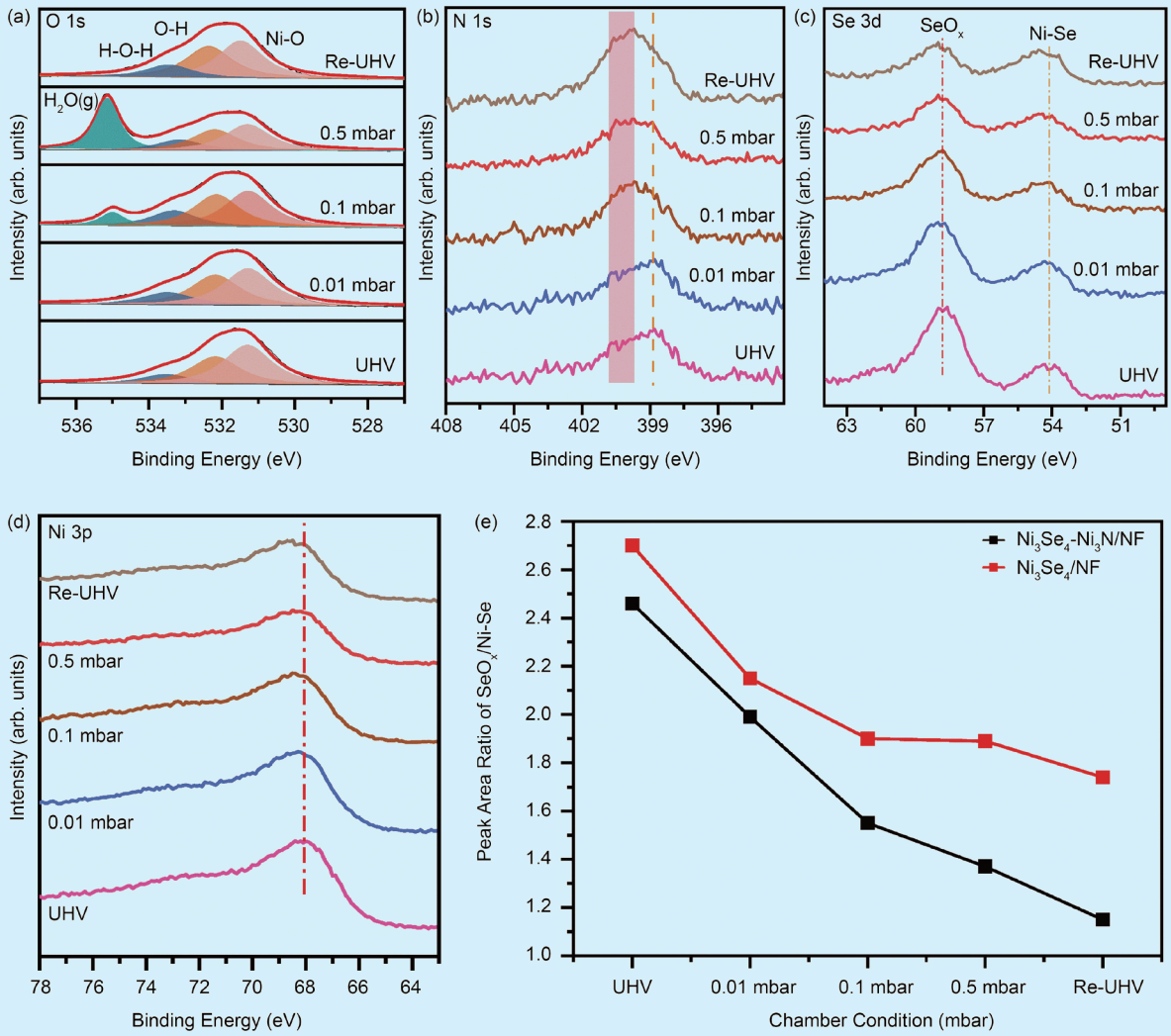

Fig. 3: Water adsorption characterization using NAP-XPS: high-resolution XPS (HR-XPS) of (a) O 1s, (b) N 1s, (c) Se 3d, and (d) Ni 3p for the Ni_3Se_4-Ni_3N catalyst at different water pressures, and (e) areal ratio of SeO_x/Ni-Se peaks, determined from Se 3d spectra at various surface water coverages. [Reproduced from Ref. 2]

analyses clearly demonstrated a pronounced HSPE on the metastable Ru/Hex-HfO_2 surface, while it was absent on the stable Ru/M-HfO_2 oxide. Due to this pronounced spillover activity, the metastable Ru/Hex-HfO_2 exhibited superior acidic hydrogen evolution reaction (HER) performance, achieving a high mass activity of 14.37 A mg_{Ru}^{-1} at an overpotential of 30 mV.

Recent studies have increasingly recognized the HSPE as a key design principle for accelerating HER kinetics. Bing Joe Hwang (National Taiwan University of Science and Technology) and his collaborators recently developed a dual-site Ni_3Se_4–Ni_3N catalyst with abundant heterointerfaces.[2] In this system, the Ni_3N substrate enhances water dissociation, increases hydrogen adsorption on the catalyst surface, and promotes hydrogen spillover to the Se sites of Ni_3Se_4, collectively boosting HER performance. This work demonstrates that the HSPE can be utilized to overcome the inherently sluggish water dissociation of transition metal selenides by integrating them with nitrides through heterointerface engineering while still leveraging the favorable electronic properties of these materials.

The electronic structure and atomic coordination of the materials were characterized using XPS and X-ray absorption spectroscopy (XAS) at beamlines **TLS 24A1** and **TLS 17C1** of the NSRRC. These analyses revealed strong interfacial charge transfer and an optimized electronic configuration in the tailored material. *In-situ* near ambient pressure XPS (NAP-XPS) measurements (**Fig. 3**) under varying water pressures further confirmed that the nitride surface exhibits enhanced water adsorption and dissociation, resulting in increased surface-adsorbed hydrogen atoms (H*). These H* species migrate to electron-rich Se sites, where they combine and release H_2 through a hydrogen spillover mechanism. The pronounced interfacial charge transfer and charge localization at the Se centers promote this spillover process. Consequently, the engineered catalyst demonstrates outstanding alkaline HER performance, requiring only ~60 mV overpotential to reach 10 mA cm^{-2} and maintaining stable operation at higher current densities.

Together, these studies provided compelling evidence that HSPE is highly structure-dependent and can be effectively activated through phase or interface engineering. Shao and his co-workers demonstrated that metastable Hex-HfO_2 serves as an efficient spillover-active substrate when combined with Ru nanoclusters, enabling exceptional acidic HER performance. By contrast, Hwang and his co-workers used a Ni_3N/Ni_3Se_4 heterointerface to facilitate hydrogen spillover, overcoming kinetic limitations of selenide materials and achieving outstanding alkaline HER activity. These findings suggest that HSPE is a promising strategy for controlling multiple intermediate steps in HER and other hydrogenation reactions. Incorporating HSPE into catalyst design allows researchers to optimize rate-limiting steps, improve catalytic efficiency, and reduce precious metal loading. Ultimately, these advances may accelerate the development of high-performance, cost-effective hydrogen production technologies, contributing to the realization of a sustainable hydrogen economy. (Reported by Dessalew Dagnew Alemayehu and Chia-Hsin Wang)

This report features the work of Qi Shao and his collaborators, published in Adv. Mater. ***37****, 2415978 (2025); and the work of Bing Joe Hwang and his collaborators published in J. Am. Chem. Soc.* ***147****, 16047 (2025).*

TPS 44A Quick-scanning X-ray Absorption Spectroscopy
TLS 17C1 EXAFS
- XANES, EXAFS
- Materials Science, Catalysts

TLS 24A1 XPS, UPS, XAS, APXPS
- HR-XPS, NAP-XPS
- Materials Science, Surface Science, Catalysts

References

1. Q. Wang, J. Chen, S. Chen, D. Zhou, Y. Du, Y. Ji, Y. Xiong, J. Ke, W. Zhu, Y. Wang, D. Gao, W.-H. Huang, C.-W. Pao, Y. Sun, Y. Li, M. Shao, Z. Hu, X. Huang, Q. Shao, Adv. Mater. **37**, 2415978 (2025).
2. D. D. Alemayehu, M.-C. Tsai, M.-H. Tsai, C.-C. Yang, C.-C. Chang, C.-Y. Chang, E. A. Moges, K. Lakshmanan, Y. Nikodimos, W.-N. Su, C.-H. Wang, B. J. Hwang, J. Am. Chem. Soc. **147**, 16047 (2025).

Projection X-ray Microscopy: Illuminating Pathways to the Future of Energy Storage

Projection X-ray Microscopy opens a window into the hidden architecture of all-solid-state batteries, decoding how microstructure shapes performance.

To reduce air pollution, including CO, CH_4, NO_2, SO_2, Pb, and PM particles, the development and production of electric vehicles has risen in prominence, with high-capacity and safe batteries being the most important priorities. All-solid-state batteries (ASSBs) using intrinsically nonflammable solid-state electrolytes (SSEs) show promise as an alternative energy-dense storage solution due to their achievable higher energy density and improved safety. In contrast to conventional lithium-ion batteries, which benefit from facile ion transport *via* infiltration of liquid electrolytes into porous electrodes, ASSBs require physical contact between solid materials to facilitate the electrochemical reaction. Ideally, all components in ASSBs should exhibit fully densified microstructures that lack any porosity to maximize volumetric energy density. However, in practice, the mismatch in particle sizes and mechanical properties of materials induces unavoidable porosity or nonideal tortuosity within ASSBs. Either formed in the initial fabrication process or during battery operation due to volume changes of cathode/anode materials, the pores and gaps in the microstructure can lead to contact loss and propagation of fractures/cracks. Contact loss of active material reduces utilization, thus leading to lower reversible capacity and capacity loss. Meanwhile, voids and fracture formation within the microstructure could also lead to structural degradation or cell failure due to the disruption of ion percolation pathways. Thus, scaled-up tomography techniques will improve the understanding of ASSBs, elevating the technology's potential commercially. To quantitatively investigate the internal microstructure and its evolution within ASSBs during fabrication and cycling, three-dimensional (3D) micro-computed tomography and reconstruction techniques are essential.[1–3]

Ying Shirley Meng (University of Chicago, University of California San Diego, and Argonne National Laboratory, USA) and her team utilized **TPS 31A** projection X-ray microscopy (PXM) 3D tomography

at the NSRRC for structural analysis of ASSB at a pouch cell scale.[1] PXM tomography is a rapid (< 30 min), high resolution (1–26 μm) and large field of view (0.7–7 mm) technique for visualizing and quantifying key microstructural features, including overhang, porosity, contact loss, active surface area, and tortuosity in ASSB pouch cells. Moreover, PXM, as a nondestructive imaging technique allowing for *in situ* and *operando* characterization, can probe the internal microstructure of ASSBs without disassembling batteries. With the recent progression in ASSBs toward larger cell formats, analyzing the bulk microstructure of individual components is essential for gaining deeper insights into their electrochemical performance. In this work, they probed the microstructure of the ASSBs using the absorption contrast imaging mode of PXM. The demonstration of microstructure and quantitative analysis of the components within the argyrodite sulfide-based ASSB pouch cell, including μ-Si anode and $LiNi_{0.8}M_{0.1}Co_{0.1}O_2$ (NMC811) composite cathode, is shown in **Fig. 1**.

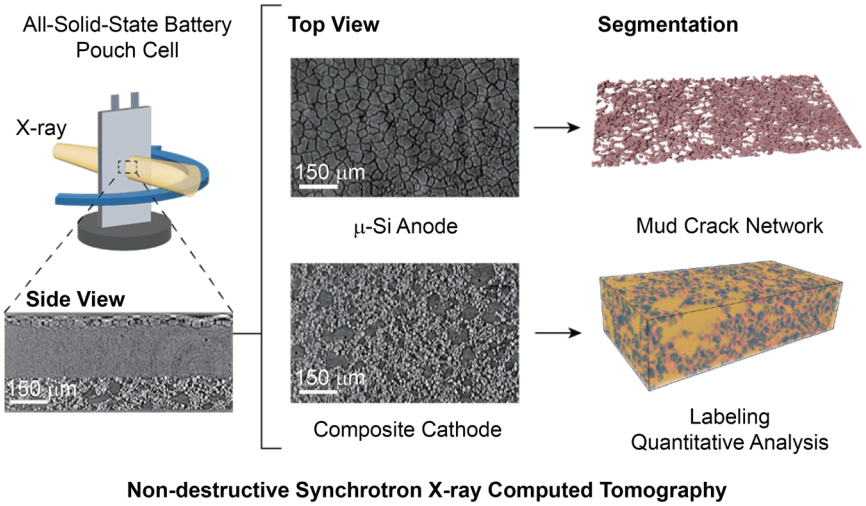

Fig. 1: PXM microstructure and quantitative analysis of the whole cell, μ-Si anode, and NMC811 composite cathode in ASSB pouch cell. [Reproduced from Ref. 1]

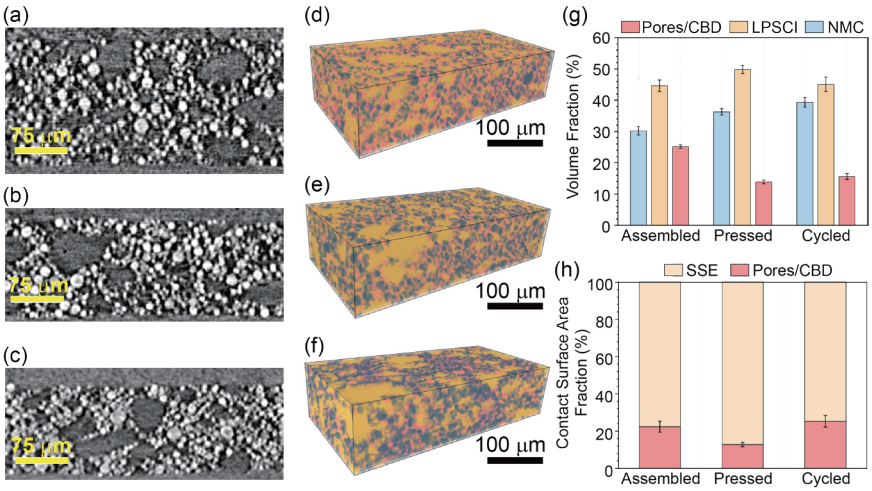

Fig. 2: Microstructure and quantitative analysis of composite cathode in pouch cells in different states: assembled, pressed, and cycled. The cross-section xy slice of (a) assembled, (b) pressed, and (c) cycled pouch cells showing the composite cathode. 3D segmented model of (d) assembled, (e) pressed, and (f) cycled pouch cells. In the 3D models, SSE is shown in yellow, NMC811 in blue, and pores/CBD in light red. (g) Volume fraction of each component within the composite cathode in different samples; (h) Contact surface area fraction of the active cathode material in the cathode composite electrode. [Reproduced from Ref. 1]

The quantitative analysis includes three stages: before cold isostatic pressing (CIP) at 500 MPa, referred to as "assembled"; after the CIP process, referred to as "pressed"; and post-C-rate test cycling at 5 MPa, referred to as "cycled". The microstructure of the three components, namely Si anode, SSE separator, and NMC811 composite cathode, during the three stages has been illustrated in detail. Specifically, the mud-crack network of the Si anode, porosity of the separator, and volume fraction and contact surface area fraction of the NMC811 composite cathode were characterized. The microstructure, volume fraction and contact surface area fraction of the NMC811 composite cathode are shown in **Fig. 2**. Cross-sectional (xy slice) PXM images provide a detailed view of the composite cathode microstructure (**Figs. 2(a)–2(c)**). Differences in X-ray absorption enable the precise identification of its components: the bright spherical particles correspond to NMC811, the gray regions represent the $LiPS_5Cl$ (LPSCl) separator, and the darkest areas represent the carbon binder domain (CBD), a mixture of pores, vapor-grown carbon fiber, and polytetrafluoroethylene (PTFE). The composite cathode electrode had an initial thickness of 180 μm within the assembled cell, which decreased to approximately 130 μm after the CIP process in both the pressed and cycled cells.

Figures 2(d)-2(f) for the segmentation results of the three stages show Pores/CBD, NMC811, and LPSCl as light red, blue, and yellow, respectively. The quantitative analysis of porosity for assembled, pressed, and cycled cells are 25.1, 13.8, and 15.6 vol%, respectively. The increased porosity of cycled compared to pressed cells could be attributed to the volume change

and potential particle cracks during charge/discharge processes of NMC811, creating gaps/voids in the microstructure that lead to the loss of physical contact, higher tortuosity, and charge transfer impedance, as well as lower active material utilization. Another important parameter governing the ASSBs' performance is the physical contact between the various composite components. **Figure 2(h)** compares the surface contact area of NMC811 particles within the composite cathode among the three samples. The fraction of the surface area of contact (between the NMC811 and SSE) of the assembled cells is 77.6%, which increased to 88.9% in pressed cells, and later decreased to 83.3% in cycled cells. The growth of the active surface area in pressed cells shows that the applied isostatic pressure compressed the pores and facilitated better physical contact between NMC811 and the SSE. This is imperative to maintain ionic transport and ensure better cathode active material utilization, namely higher reversible capacity. Meanwhile, the decline of the active surface area in cycled cells implies void formation, resulting from the volume change of NMC811 and plastic deformation of LPSCl.

To further explore the correlation between microstructure and electrochemical performance, significant efforts have been devoted to the computational modeling of ASSB degradation. The superiority of PXM tomography lies in its ability to access and analyze the microstructure and morphology of ASSBs with exceptional detail. PXM imaging and segmentation provide quantitative insights into critical microstructural information. Leveraging the nondestructive nature of tomography, the 3D PXM models at different states of charge or cycles can be integrated with computational modeling to understand the chemo-mechanical degradation mechanism of ASSBs. PXM-segmented 3D models provide true-to-life geometry and authentic microstructure representation, offering a practical starting point for advancing simulation and modeling. **Figure 3** outlines a proposed multiphysics simulation workflow that incorporates PXM reconstructed 3D microstructures to study ASSB degradation mechanisms. The approach starts with reconstructing the measured PXM slices to obtain realistic 3D models of ASSB microstructures. Subsequently, the surface representation of each segmented particle and features can be easily converted using commercially available software.

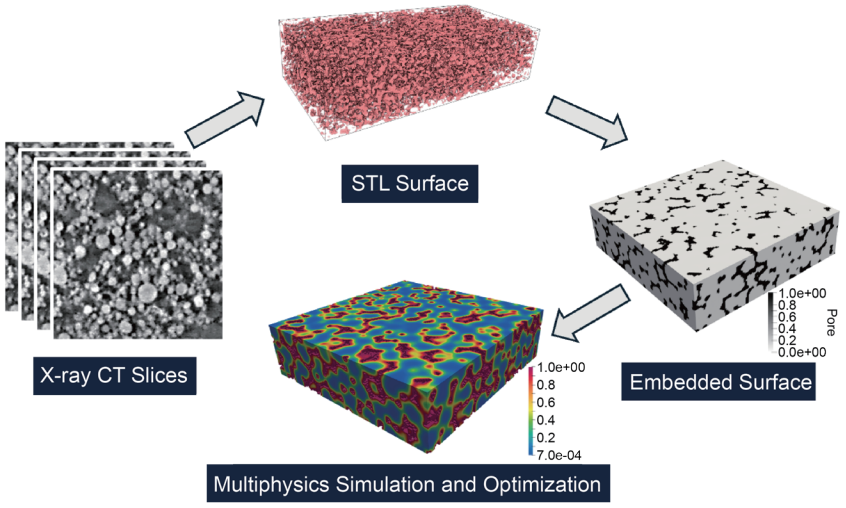

Fig. 3: Multiphysics simulation workflow using realistic PXM reconstructed 3D models. Schematic showing workflow of using real 3D PXM models for multiphysics simulation in four steps: obtaining PXM slices, generating surface mesh file, regularizing noisy surface representations, and multiphysics simulation and optimization for ASSB degradation mechanism study. The colormaps in the simulation model represent different phases including particles, the void, and the regularized transition zone. [Reproduced from Ref. 1]

In summary, PXM offers quantitative insights into the ASSB microstructure, including (1) porosity of individual components, (2) particle size distribution for tortuosity analysis, (3) volume fraction in the composite cathode, (4) contact surface area between active cathode materials and voids or solid state electrolytes, and (5) delamination at the Cu current collector and the Si anode interface. PXM investigation on ASSBs at the pouch cell level provides industry-relevant insights, leading the design and engineering of robust and high performance ASSBs for practical applications. (Reported by Yen-Fang Song)

This report features the work of Ying Shirley Meng and his collaborators published in ACS Energ. Lett. ***10****, 3459 (2025).*

TPS 31A Projection X-ray Microscopy

- PXM
- Chemistry Engineering, Materials Science, Green Sustainable Chemical Process

References

1. C.-J. Huang, J. A. S. Oh, M. Vicencio, T. Hu, H. Yang, J. N. Burrow, Y.-F. Song, G.-C. Yin, P. Shevchenko, K. M. Wiaderek, B.-J. Hwang, Y. S. Meng, ACS Energ. Lett. **10**, 3459 (2025).
2. H. Chen, H.-W Liu, Y.-C. Lu, P.-J. Yu, C.-H Liao, C.-C. Wang, T.-S. Chan, H.-S. Sheu, P.-Y. Chang, J.-L. Chen, S.-C. Haw, G.-C. Yin, Y.-F. Song, C.-W. Pao, N.-L. Wu, Chem. Eng. J. **519**, 165314 (2025).
3. H.-W Liu, H. Chen, S. Thi, P.-J. Yu, J.-L. Chen, C.-W. Pao, P.-Y. Chang, S.-C. Haw, Y.-F. Liao, Y.-C. Shao, G.-C Yin, Y.-F. Song, S.-K. Parthasarathi, Y.-T. Weng, N.-L. Wu, Compos. Pt. B **293**, 112133 (2025).